



**HAL**  
open science

## Efficient 2D ray-tracing method for narrow and wide-band channel characterization in micro-cellular configurations

Pierre Combeau, Lilian Aveneau, Rodolphe Vauzelle, Yannis Pousset

► **To cite this version:**

Pierre Combeau, Lilian Aveneau, Rodolphe Vauzelle, Yannis Pousset. Efficient 2D ray-tracing method for narrow and wide-band channel characterization in micro-cellular configurations. IEE Proceedings Microwaves Antennas and Propagation, 2006, 153 (6), pp.502-509. 10.1049/ip-map:20045142 . hal-00348480

**HAL Id: hal-00348480**

**<https://hal.science/hal-00348480v1>**

Submitted on 19 Dec 2008

**HAL** is a multi-disciplinary open access archive for the deposit and dissemination of scientific research documents, whether they are published or not. The documents may come from teaching and research institutions in France or abroad, or from public or private research centers.

L'archive ouverte pluridisciplinaire **HAL**, est destinée au dépôt et à la diffusion de documents scientifiques de niveau recherche, publiés ou non, émanant des établissements d'enseignement et de recherche français ou étrangers, des laboratoires publics ou privés.

# Efficient 2D Ray-Tracing Method for Narrow and Wide-band Channel Characterization in Micro-cellular Configurations

Pierre Combeau, Lilian Aveneau, Rodolphe Vauzelle and Yannis Pousset  
SIC, FRE CNRS 2731

SP2MI, Bd Marie et Pierre Curie, BP 30179, 86962 FUTUROSCOPE CHASSENEUIL Cedex - France  
Email: combeau@sic.univ-poitiers.fr. Phone number: (+33)5-49-49-66-17. Fax: (+33)5-49-49-65-70

**Abstract**— Channel characterization is an essential step to the development of outdoor or indoor wireless networks. Indeed, for multimedia applications, new radio mobile systems must accurately take into account channel behavior. In this paper, we propose an efficient 2D ray-tracing method to characterize the narrow and wide-band radio channels for a very large number of receivers in micro-cellular configurations. It is based on a quick pre-calculation of an exact 2D visibility graph. The proposed method follows an ITU recommendation, which advocates, for wide-band characterization, only considering the paths included in a 18 dB dynamic range of power impulse response. Contrary to the classical approach, which consists in thresholding the complete impulse response in a post-treatment, our method only computes the significant paths.

The interest of the proposed method resides in its significant computation time reduction factor, in comparison with the classical approach and this without any significant loss in accuracy. Received power and wide-band parameter maps are computed for about 40,000 receivers, in a dense urban environment, and are provided with an approximate reduction factor of 4 and 80% of null estimation error in comparison to a classical approach.

## 1. Introduction

In the near future, the market for wireless networking facilities is expected to grow considerably. The importance of new services, such as high speed data and multimedia services, which are demanding in terms of bit rate and thus bandwidth, has raised an increasing interest for wide-band applications. Since spectral resources are limited and the number of users keeps on increasing, micro-cellular systems are now a solution. These systems require an accurate knowledge of wave propagation, not only in narrow-band, but also in wide-band.

Ray-tracing methods have emerged as a highly promising procedure for providing an accurate site-specific means to obtain useful simulation results [1], [2]. Indeed with the Geometrical Optic (GO) and the Uniform Theory of Diffraction (UTD), these methods can consider all the main physical phenomena: line of sight propagation, reflection, diffraction and their combination, in order to simulate complex rays. In many realistic propagation environments, these complex rays drastically slow down the multi-path determination procedure. However, some optimization methods, such as the use of AZ buffer [3] or space-division methods [4], [5], [6] have been developed to keep computation times down to an acceptable level. Nevertheless, these solutions can remain very time-consuming when a large number of receiver locations is

considered [7]. Indeed, as they are point to point ones, the computation time is directly linked to the number of computed radio links. This justifies the interest in pre-processing the propagation environment based on a visibility graph computation [8], [9], [10], [11], [12], [7]. The principle of a visibility graph is to build, for a given transmitter location, all the spatial zones illuminated after any number of propagation phenomena. The result is represented by a tree of zones. The root is the transmitter; the first level corresponds to the zones defined after a first interaction and so on. Thus, to build all the paths received in a particular location, we only need to identify the zones, including the receiver, and to follow up the tree of zones until the root for each of them. Each path through the tree corresponds a received path. Their electromagnetic characteristics (magnitude, phase, polarization...) are provided by a classical method based on the Geometrical Optic and the Uniformed Theory of Diffraction [13].

In [10], a polar sweep line technique is used to achieve the visibility graph computation. This method provides an exact graph but still requires a lot of time consuming intersection tests for its building. In [12], Athanasiadou uses the image theory and the illumination zone concept to compute the visibility graph, and in [7] Hoppe establishes a pseudo visibility tree between different faces or edges center points. In these two cases, the result is not exact, so intersection tests are necessary between the next interaction point and the receiver to validate the paths, so these optimisation structures are not optimal.

In this paper, we propose a technique in order to achieve an efficient ray-tracing procedure using an exact visibility graph. This model is particularly adapted to narrow and wide-band channel characterization for a high number of receivers. We first explain how to compute the visibility graph efficiently. Then, we suggest a technique to optimize ray-tracing for the channel characterization of a large number of receivers, based on a visibility graph.

The presentation of this work is organized as follows. In section 2, the authors describe the principle leading to the creation of an exact visibility graph. Section 3 proposes the efficient use of a ray-tracing model based on image theory [4] and using the visibility graph, in the case of a large number of receivers. The objective is to provide an efficient solution

for channel characterization and, in particular, in the case of the procedure recommended by the ITU [15]. Because, this recommendation advocates a power delay profile dynamic range equal to 18 dB [15] for the estimation of the wide-band parameters, the proposed solution only allows computation of the paths included in this dynamic range.

Finally, the evaluation of the proposed method in terms of computation time and accuracy is presented in section 4. One of the interests of this method is to produce, in a very short time, maps of wide-band parameters in large areas such as downtown Paris. These representations are equivalent to a radio coverage forecast, but for either the rms delay spread or the coherence bandwidth channel forecasts.

## 2. Exact 2D visibility graph

A visibility graph is a data structure that encodes the spatial zones illuminated after any number of interactions. It has the form of a tree of zones. Each zone has several characteristics, such as its contour and its virtual point source. Such a graph can be used to determine all the received paths in any particular location, by scanning it. Obviously, if it is computed in a pre-process step, it should lead to large computation time improvements when many receiver locations are considered.

This technique is very efficient compared to a classical ray-tracing. It avoids carrying out all the expensive intersection tests used to search for the objects which are reached by the rays between a transmitter and the receivers. With a visibility graph, these tests become useless, since all the possible paths reaching the receiver are directly defined.

There are several ways of computing a visibility graph [10], [12], as previously presented in section 1. Here we propose a new method that makes it possible, contrary to the previous techniques, to efficiently calculate a precise one.

The principle is based on a recursive algorithm. At each step, we cut the studied environment into several zones according to an electromagnetic interaction: line of sight for the first tree level, reflection or diffraction for the next ones. It is important to note that, for implementation simplicity and robustness, we define each zone contour as a triangle or a quadrangle.

Let us present this algorithm with an example. The transmitter location is first associated to the tree root. At the first recursive step, the visibilities from the root are computed. They represent the line of sight phenomenon. To do this we define four triangles, as shown in figure 1 (a): one of their vertices is  $T_x$ , while the others are the corners of the scene. Then, these four zones are cut, in order to take into account the surrounding buildings. As shown in figure 1 (b), this leads to nine exact visibility zones. The recursive algorithm continues for each such zone. It lets us compute their children according to an electromagnetic interaction: reflection or diffraction. For instance, figures 1 (c) and (d) show respectively the reflected zones from zone 2, and the diffracted ones from D1. This recursive algorithm ends when the given number of interactions has been processed.

The main parameter of any visibility graph computation is the number  $N = N_R + N_D$  of considered electromagnetic

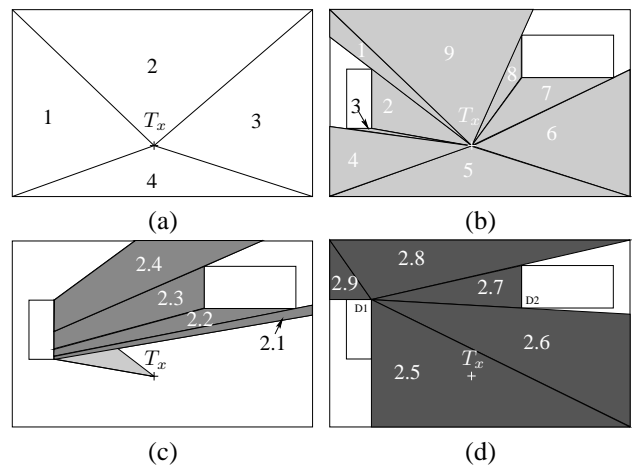


Fig. 1. (a) initialization, (b) computation of visibility zones, by considering the buildings, (c) example of a reflected zone computation, (d) example of a diffracted zone computation

interactions ( $N_R$  reflections and  $N_D$  diffractions); obviously,  $N$  gives its maximum depth.

Let us remember that the graph computation is made only once, wherever the receivers are located in the studied area. Clearly, for a high number of receivers, this makes it possible to greatly reduce the computation time for searching and building the paths. However, this algorithm efficiency is based on two key points: the strategy for cutting the zones up around the surrounding buildings, and the memory consumption for a high number of electromagnetic interactions. We use two techniques to solve these problems.

The first one is based on the discrete mathematics, and consists in using a discrete grid [16], where each cell contains a list of included buildings: in a preprocessing step, a discrete grid is applied on the environment, and the grid cells intersecting the environment objects (buildings) are so identified. This step is created by calculating of each building's "super-cover". For this, we consider the grid cells as pixels of a classical digital image. In this way, we can define the super-cover of a 2D line  $\Delta$  of equation  $ax+by+c=0$ , where  $(a, b, c) \in \mathbb{R}^3$  are the line coefficients. It is composed by all the pixels between two 2D lines  $D'$  and  $D''$ , defined by:

$$D' : a(x + \frac{1}{2}) + b(y + \frac{1}{2}) + c = 0 \quad (1)$$

$$D'' : a(x - \frac{1}{2}) + b(y - \frac{1}{2}) + c = 0 \quad (2)$$

In other words, the supercover of  $\Delta$  is composed by all the pixel  $(x, y)$  given by the following double inequality:

$$-\frac{([a] + [b])}{2} \leq ax + by + c \leq \frac{([a] + [b])}{2} \quad (3)$$

where  $[ \ ]$  defines the integer part function.

From this, we can identify for each line its extrema on X-axis and Y-axis. So, the problem of calculating intersection between two lines is reduced to compare different pixels coordinates. In this way we can quickly find all the intersections between a zone and the scene's objects. Readers will find more details on this method in [16], where we show it is very efficient.

The second technique consists in reusing different sub graphs already calculated after diffraction [10]. For instance, the sub graph created from diffraction at D2 is computed a first time from the visibility zone 7. It can be reused from the reflected zone 2.3, from the diffracted zone 2.7, and so on. This drastically reduces the memory storage requirements, as shown by our experiment.

### 3. Visibility graph and channel characterization

The channel characterization is based on the power delay profile (PDP) determination for each radio link. The proposed method is directly related to an ITU recommendation on wide-band channel characterization [15]. It advocates using for characterization, only those PDP paths included in a dynamic range equal to 18 dB.

So, we propose an efficient use of the visibility graph consisting in only building the paths in the given dynamic range, instead of removing the non-significant paths by a classical PDP post processing. This method, called Significant Paths Search (SPS), can provide a considerable computation time gain as shown in section 4. In order to precisely evaluate such a computation time reduction, we have to compare it with a more naïve solution, which consist in calculating all the paths. This solution, noted Full Path Search method (FPS), is defined in the same way as SPS, but without taking into account the ITU recommendation.

The general principle of the proposed method consists in following up the visibility graph (since it is a tree) only for the zones which correspond to significant paths. Indeed, the simplest way is to test all the zones of the graph. Since the number of zones is generally very high (several millions), and since the probability for each zone to contain the receiver is very low, this will generate large computation times for a low number of resulting paths.

So, we split up this process into two stages :

- A second 2D discret grid is used to reduce the inclusion tests. Each cell contains a list of included zones. For the SPS algorithm, and for each grid cell, the zone list is sorted by descending path loss, in order to respect the ITU recommendation.
- Then, for each receiver location, the tree is followed up to its root in order to compute the paths.

Let us now describe these two stages for the FPS algorithm. In the first one, an algorithm based on discrete geometry is used, as in [16]. All the visibility graph zones are plunged into a discrete grid, using their super-covers in a similar way to the plunging of buildings (*cf.* section 2).

In the second one, and for each receiver location, the inclusion tests are limited to the zones included into the cell surrounding the receiver. Then, the PDP paths are directly computed. Since the zones used for the inclusion tests have a high probability of containing the receiver, this method leads to a considerable reduction in terms of computation time.

Note that the discrete grid resolution has to be defined in order to optimize the trade-off between the computation times of the plunging and the inclusion tests. Our experiments show that a good compromise is usually a grid size of 30x30 for the FPS algorithm.

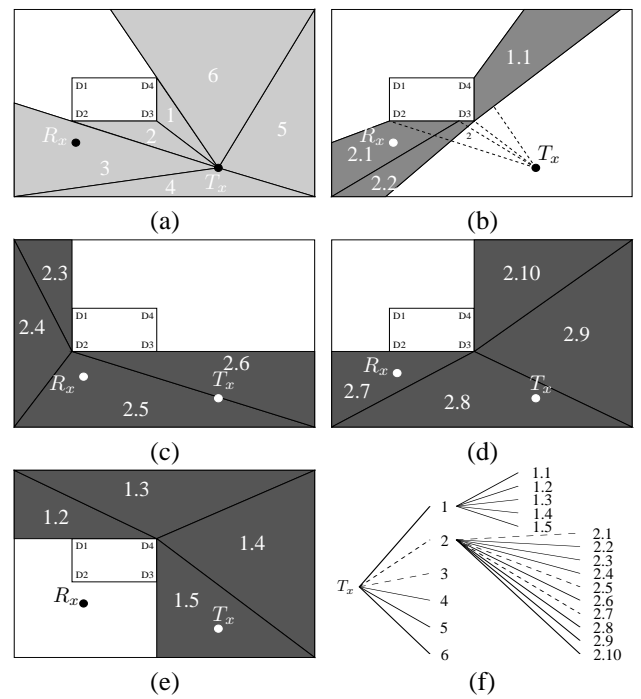


Fig. 2. (a) visibility zones, (b) reflected zones from (D2D3) and (D3D4), (c) diffracted zones from D2, (d) diffracted zones from D3, (e) diffracted zones from D4, (f) the visibility graph for 1 reflection and 1 diffraction

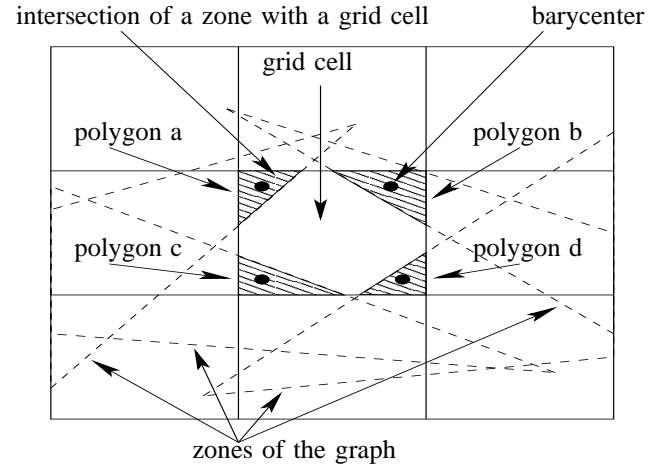


Fig. 3. Computation of the intersection polygons between four zones and a grid cell

Don't forget that, for path calculations, and unlike ray-tracing methods without an exact visibility graph, no visibility tests are required. This lets us reduce computation time once more. As illustration of the FPS algorithm, figure 2 (f) shows the computation of the different paths (in dashed lines) by traversing the graph from a receiver  $R_x$  – depicted in figures 2 (a) to (e) – to a transmitter  $T_x$ .

For the SPS algorithm, the first stage is slightly enhanced: For each cell of the grid, the zones are sorted by decreasing path loss. In order to maximize accuracy, the path losses are computed at the barycenter of the intersection, between the cell and the zones.

This is illustrated on figure 3 example, where 4 zones are

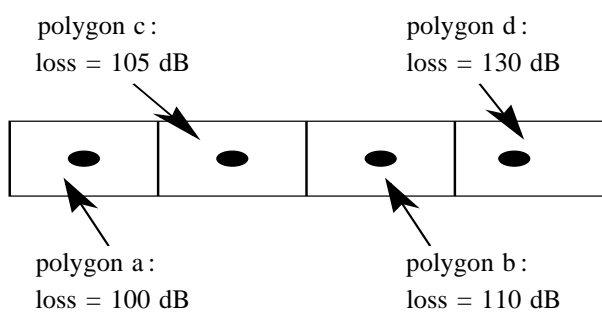


Fig. 4. Polygons classification for the center grid cell

contained in the center grid cell. This process results in a vector containing the polygons sorted by their associated path loss, as depicted in figure 4.

For the SPS algorithm, the second stage becomes more complex. It is depicted in figure 5. It lets us determine efficiently the received paths in a given dynamic range.

Let us describe some details of this algorithm:

- As soon as a first polygon including the receiver is found, its associated path reaching the receiver is computed and added to the PDP. This path loss is temporarily stored, as the beginning reference for the dynamic range.
- The algorithm continues with the polygons containing the receiver sorted next. Each corresponding path in the dynamic range is added to the PDP. When necessary, the beginning reference for the dynamic range is modified. This process stops as soon as a path loss is found outside the dynamic range. Indeed, because the polygons have been sorted, all the following polygons should give larger losses, therefore outside the dynamic range.

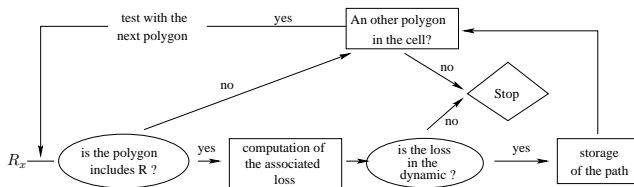


Fig. 5. Algorithm for finding the significant paths

Note that the estimation, due to the calculation at each zone's barycenter, can lead to missing some paths. To solve this problem, a parametrized security margin is added to the ITU recommended dynamic range. Even if more polygons are tested, only those paths which are strictly included in the initial dynamic range are kept.

A study, which is not presented here, indicates that the grid resolution used in the first stage modifies the computation time, but has no impact on accuracy. This study has concluded on an optimal resolution of 8x8. Readers will find more details about this study in [14].

So with the SPS algorithm an important reduction in computation time should be provided, since only the paths included in the given dynamic range are computed (Note that there is any limitations/constraints about the dynamic range value).

The evaluation of this reduction and loss in accuracy are two of the objectives of the next section.

#### 4. Performance evaluation

The purpose of this section is to evaluate performances of the SPS method in terms of accuracy and computation time. The objectives are therefore to check if this method lets us correctly eliminate the non-significant paths, and if it leads to a computation time reduction. To do this, we have to use a reference model which provides a complete impulse response, with the significant and the non-significant paths according to the ITU [15]. This complete impulse response will then be thresholded in function of the fixed dynamic range, in a post-treatment. Finally, we have just to compare the different parameters calculated from these two different impulse responses: the first provided by the reference model after thresholding, and the second provided by the SPS method.

The FPS method has been chosen as the reference model, because it lets us compute all the paths between the base station and a receiver. In the same way as that of all ray-tracing methods, its main parameter is the combination of electromagnetic interactions to be considered for propagation computation. Rather than considering any combination, we suggest using measurements, as shown in the next paragraph. Next the accuracy study of the SPS method is presented.

This study is carried out in a dense urban environment: the roundabout of l'Arc de Triomphe in Paris, France. The dimensions of this environment are 1162x1364 meters. It includes 813 buildings with 9,516 vertical edges and as many 2D vertexes. The simulated system is micro-cellular with the transmitter antenna below the average height of the rooftop. The full environment and the mobile route corresponding to the measured signal are shown in figure 6. The length of the mobile route is about five thousands meters and the spatial step between two measure points of about three meters. For measurement, we have used dipole antennas and Rohde&Schwarz field strength receiver.

#### 4.1. Interactions combination choice

Figure 7 shows the evolution of measured and simulated (with FPS) received power on the mobile route at 2 GHz.

We propose three simulations which respectively correspond to a combination of interactions equal to 4R-1D, 10R-1D and 6R-2D, where R and D indicates the number of Reflections and Diffractions which have been taken in account. Note that since the dynamic range of the measured signal is high, some receivers can receive no path. This case takes place between 2500 and 2700 m with 4R-1D for example, where the estimated received power is fixed at 0 dBm. The choice consisting in fixing the received power at 0 dBm for the non-reached receivers is absolutely arbitrary. Table I indicates, for each combination, the mean error and the standard deviation of the error between each FPS simulation and measurement. Obviously, we do not take into account the receivers located between 2500 and 2700 m. Furthermore, more complex combinations as 10R-1D or 6R-2D allow to cover them but

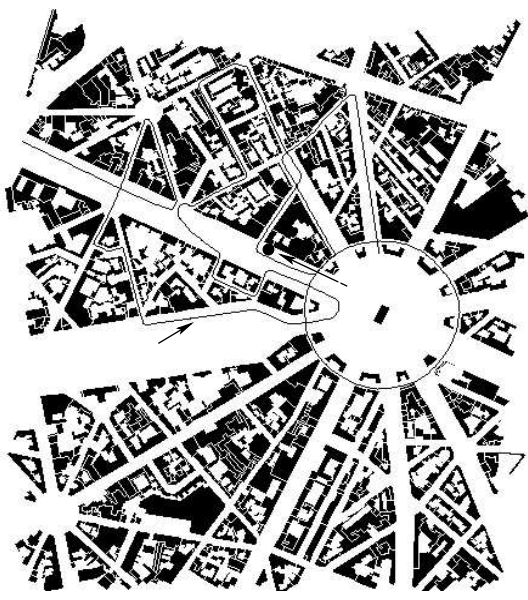


Fig. 6. Studied configuration and mobile route

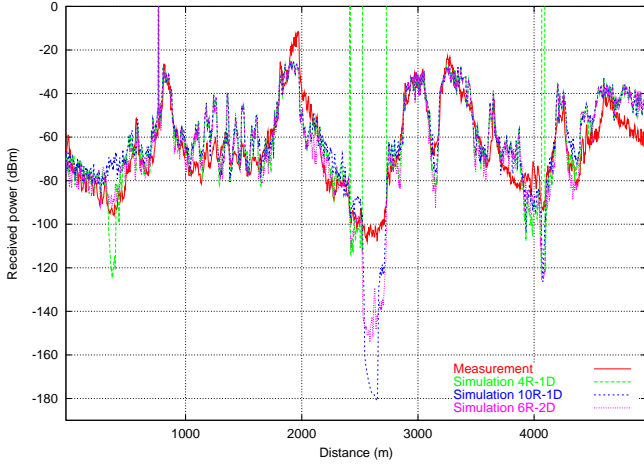


Fig. 7. Comparison between measured and simulated (with FPS) received power along the mobile route of figure 6

with a very bad estimation. Note that for all simulations, the environment objects have been considered in concrete, and the corresponding electrical properties have been fixed at 0.9 for the relative permittivity and  $0.1 S.m^{-1}$  for the conductivity, as it is shown in the fourth column of table I.

TABLE I

ACCURACY STUDY IN FUNCTION OF INTERACTIONS COMBINATION

Interactions combination	$\mu$ (dB)	$\sigma$ (dB)	(relative permittivity, conductivity)
4R-1D	1.59	9.53	(9, $0.1 S.m^{-1}$ )
10R-1D	4.07	8.87	(9, $0.1 S.m^{-1}$ )
6R-2D	0.99	9.25	(9, $0.1 S.m^{-1}$ )

Note also that we use the classical Fresnel reflection coef-

ficients given by :

$$R_{//} = \frac{n_i \cos \theta_t - n_t \cos \theta_i}{n_i \cos \theta_t + n_t \cos \theta_i} \quad (4)$$

$$R_{\perp} = \frac{n_i \cos \theta_i - n_t \cos \theta_t}{n_i \cos \theta_i + n_t \cos \theta_t} \quad (5)$$

where  $\theta_i$  and  $\theta_t$  are respectively the incident and transmission angles, and  $n_i$  and  $n_t$  the refraction indices of the air and the reflecting object. Finally, the used diffraction coefficients are those given by Kouyoumjian and Pathak [13] :

$$D_{//,\perp}(L, \phi, \phi_0, n) = D_1 + D_2 + R_{//,\perp}(D_3 + D_4)$$

where  $D_1$ ,  $D_2$ ,  $D_3$ , and  $D_4$  are given by :

$$D_1 = \frac{-e^{-j\frac{\pi}{4}}}{2n\sqrt{2\pi k} \sin \beta_0} \cot \left[ \frac{\pi + (\phi - \phi_0)}{2n} \right] F [kLa^+(\phi - \phi_0)] \quad (6)$$

$$D_2 = \frac{-e^{-j\frac{\pi}{4}}}{2n\sqrt{2\pi k} \sin \beta_0} \cot \left[ \frac{\pi - (\phi - \phi_0)}{2n} \right] F [kLa^-(\phi - \phi_0)] \quad (7)$$

$$D_3 = \frac{-e^{-j\frac{\pi}{4}}}{2n\sqrt{2\pi k} \sin \beta_0} \cot \left[ \frac{\pi + (\phi + \phi_0)}{2n} \right] F [kLa^+(\phi + \phi_0)] \quad (8)$$

$$D_4 = \frac{-e^{-j\frac{\pi}{4}}}{2n\sqrt{2\pi k} \sin \beta_0} \cot \left[ \frac{\pi - (\phi + \phi_0)}{2n} \right] F [kLa^-(\phi + \phi_0)] \quad (9)$$

and  $F(x)$  is the transition function :

$$F(x) = 2j\sqrt{x} e^{jx} \int_{\sqrt{x}}^{\infty} e^{-jt^2} dt \quad (10)$$

The analysis of these results shows that the accuracy evolution is weak according to the interaction combination. So we retain 4R-1D because its computation time is the smallest. Indeed, the more numerous the interactions, the longer the computation time. Nevertheless, note that one must not focus on the values in table I. They are given for illustration only. In the next section, for the accuracy validation of the SPS method, the reference is not the measurement, but the FPS method which gives the same accuracy as other 2D ray-tracing models. The relative imprecision of FPS results is due to the well-known problems such as environmental data imprecision, electrical properties of materials and the influence of vegetation.

## 4.2. Narrow and wide-band accuracy study

Let us clarify some words. From this point, we will talk about “narrow-band study” for the study of received power, and about “wide-band study” for the study of the PDP and parameters calculated from it (such as rms delay spread for instance).

Since we have determined the reference result, (FPS method with parameters 4R-1D), we can now evaluate the accuracy of the Significant Path Search (SPS) method. You must remember that to do this, the estimated results provided by SPS are compared with those estimated by FPS, after a thresholding process. This one consists in only keeping the paths included in a dynamic range equal to 18 dB, as recommended by the

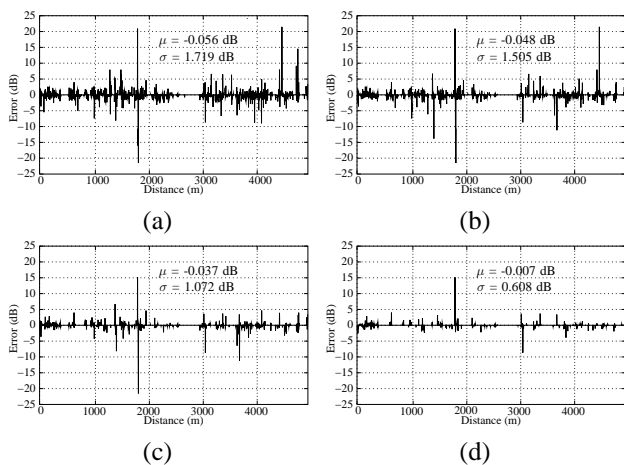


Fig. 8. Errors of estimation between FPS and SPS simulations for a: 2 dB margin (a), 5 dB margin (b), 10 dB margin (c), 15 dB margin (d)

ITU. Note that we present the results for different security margins.

Figure 8 presents the evolution of the estimation error (on received power) between SPS and FPS, along the mobile route for 4R-1D. More precisely, the figures 8 (a), (b), (c) and (d) respectively correspond to a security margin equal to 2, 5, 10 and 15 dB. It is noticeable that the error significantly decreases according to the security margin increase. Indeed, the average error goes from -0.056 dB for a 2 dB margin, to -0.007 dB for a 15 dB one, whereas the standard error deviation goes from 1.719 dB for a 2 dB margin to 0.608 dB for a 15 dB one. To conclude, the SPS algorithm leads to very accurate results, compared to FPS.

In order to complete this parametric study, we consider two maps showing the evolution of received power (figure 9) and rms delay spread (figure 10) in the environment of figure 6.

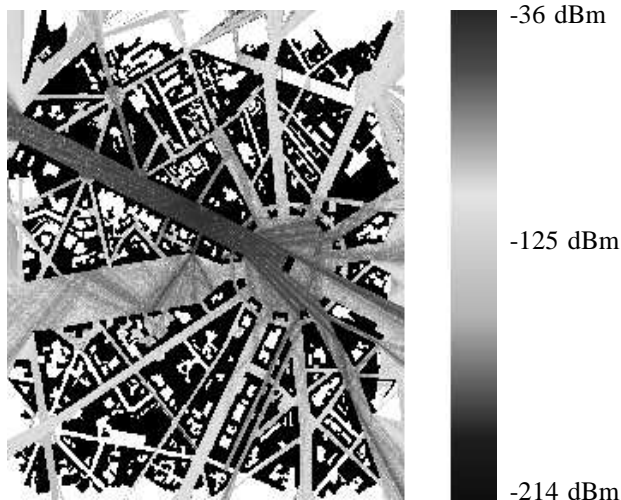


Fig. 9. Coverage zone

These maps correspond to 39,672 receiver locations with a neighboring separation of five meters, on the same scene as above.

Concerning the study in narrow-band, we present the cumu-

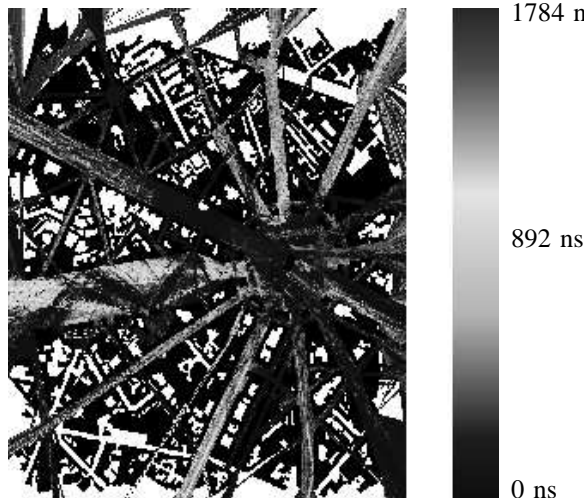


Fig. 10. Rms delay spread map

lative function of the error for the estimated received power between the two methods for different values of the security margin (figure 11). One can conclude that the estimations provided by SPS and FPS are very close, with a security margin equal to 10 and 15 dB. Indeed, for a 15 dB margin, 97% of errors are null and the 3% remaining are less than 2 dB. For a 10 dB margin, 91% of errors are null and the 9% remaining are less than 4 dB. Finally, note that even for a small margin of 2 dB, 95% of errors are less than 2 dB.

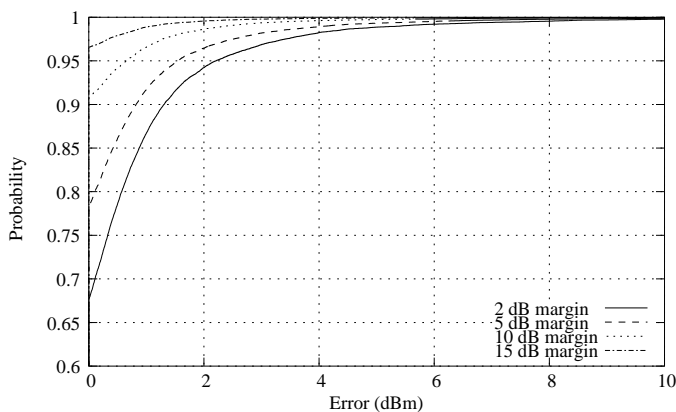


Fig. 11. Cumulative functions ( $\Phi_{1_{margin}}$ ) of the error for estimated received power

In wide-band, figure 12 shows the same curves but for the rms delay spread parameter. We can conclude in a similar way since 97% of errors are null for a 15 dB margin and, whatever the margin is, 95% of errors are always less than 60 ns which is very weak in comparison to the dynamic range (1800 ns).

### 4.3. Computation time

To complete the performance study, we present in this section the computation times of the proposed method in the environment of figure 6, which is composed of 9,516 edges and vertexes. All the computation times have been obtained with an Athlon XP 1800+. They correspond to the

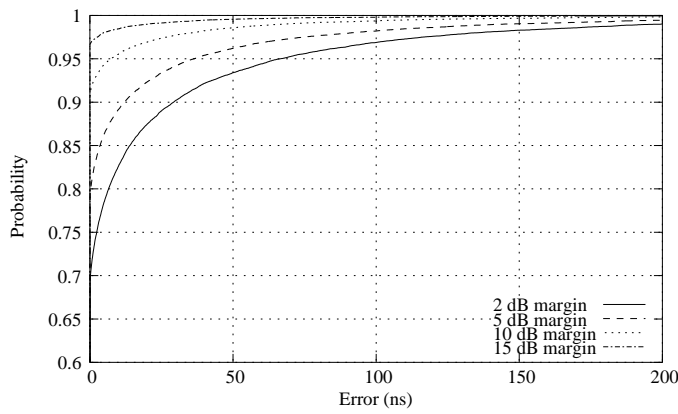


Fig. 12. Cumulative functions ( $\Phi_{2_{margin}}$ ) of the error for estimated rms delay spread

same configuration as above (39,672 receiver locations, with 4R-1D). Table II shows the trade-off between efficiency and accuracy for the SPS method in comparison to the FPS one after thresholding, according to the security margin.

For each method, this table indicates two types of information: on the one hand computation times in seconds, and on the other hand, accuracy information previously indicated related to received power and rms delay spread. The first column (pre-processing) corresponds to the visibility graph computation, and the second one to the additional time needed for a full channel characterization in the full environment. More precisely, this last time corresponds to the plunging step, the ray-tracing procedure, the calculation of the coverage zone and all the maps of wide-band parameters (mean delay, rms delay spread, coherence bandwidth at 50% and 90% -not presented in this paper-).

TABLE II  
SPS ACCURACY AND COMPUTATION TIME PERFORMANCES

	Pre-processing (s)	Path computation (s)	Received power		Rms delay spread	
			Null error (%)	$\Phi_{1_{95\%}}$ (dB)	Null error (%)	$\Phi_{2_{95\%}}$ (ns)
FPS	57 s	716 s	68%	2.2 dB	72%	68 ns
SPS <sub>2dB</sub>	57 s	165 s	79%	2.2 dB	82%	68 ns
SPS <sub>5dB</sub>	57 s	181 s	92%	0 dB	91%	0 ns
SPS <sub>10dB</sub>	57 s	210 s	97%	0 dB	97%	0 ns
SPS <sub>15dB</sub>	57 s	251 s	97%	0 dB	97%	0 ns

This table shows that the SPS method generated a great reduction in computation time, whatever the margin value is. Thus, the gain factor goes from 4.34 for a 2 dB margin to 2.85 for a 15 dB one. Considering both the number of receiver locations and the number of interactions, our ray-tracing solution becomes fast enough to be used for channel characterization, either in narrow or wide-band.

Note that the computation time reduction is obtained with a negligible accuracy degradation for narrow and wide-band channel characterization, as shown in the columns three and four in table II. Indeed, they recall some information about the SPS accuracy in comparison with the FPS ones: the null error percentage and the 95% value of the cumulative functions of

the figures 11 and 12 ( $\Phi_{1_{margin}}$  and  $\Phi_{2_{margin}}$ ). The null error percentage, for the received power and rms delay spread estimations, is always more than 70%. Moreover, 95% of the errors are, in the worst case (for a 2 dB margin), respectively less than 2.2 dB for received power and less than 65 ns for rms delay spread, which is very low in comparison with the dynamic range of the maps (figures 9 and 10).

## 5. Conclusion

For micro-cellular systems, we have presented a method (SPS) which makes it possible to characterize quickly and accurately the radio channel for a very large number of receivers, in narrow and wide-band. This method, being able to only compute the paths in a given dynamic range, constitutes an efficient solution for the ITU recommendation relative to the channel characterization. It relies on the pre-calculation of an exact visibility graph and on the plunging of its zones in a discrete grid. The plunged zones undergo an additional pre-processing consisting in sorting them in decreasing order, according to their associated losses.

To evaluate SPS performance, we have considered a naïve version (FPS) of SPS which calculates all the paths between the base station and a receiver.

The study presented has been carried out in a dense urban environment corresponding to a micro-cellular configuration. The narrow and wide-band results are provided under the form of received power (coverage zone) or rms delay spread maps. It is important to note that the method proposed lets us favor either accuracy or computation time, according to the security margin. For instance, for 40,000 receivers, the computation time reduction factor, by comparison to the naïve version, goes from 2.85 to 4.34, respectively for a 15 dB and 2 dB margin. For these same margin values, 95% of the estimation errors are respectively equal to 0 and 2.2 dB for received power and to 0 and 65 ns for rms delay spread.

In conclusion, a significant reduction time factor is obtained with a very insignificant approximation.

Finally, note that such a representation under the form of a map is interesting because one can identify some regions in the studied area, where the channel behavior is quasi-constant. Indeed, for a specific wireless system (such as UMTS), it becomes possible to predict the bit error rate of a communication with a realistic channel behavior, instead of considering normalized channels [17].

In our future work, we will focus on the extension of the approach presented, in 3D and for indoor environments, in order to study WLAN systems for example.

## References

- [1] S. Y. Seidel and T. S. Rappaport. Site-specific propagation prediction for wireless in-building personal communication system design. *IEEE-VEH*, 43:879–891, November 1994.
- [2] G. Liang and H. L. Bertoni. A new approach to 3-d ray tracing for propagation prediction in cities. *IEEE-ANT*, 46:853–863, June 1998.
- [3] F. S. de Adana, O. G. Blonco, I. G. Diego, J. P. Arriaga, and M. F. Catedra. Propagation Model Based on Ray Tracing for the Design of Personal Communication Systems in Indoor Environments. *Proc. IEEE-VEH*, vol 49, pages 2105-2112, November 2000.



- [4] M. F. Iskander and Z. Yun. Propagation prediction models for wireless communication systems. *IEEE Transactions on microwave theory and techniques*, 50(3), March 2002.
- [5] Z. Yun, M. F. Iskander, and Z. Zhang. Fast Ray Tracing Procedure Using Space Division With Uniform Rectangular Grid. *Electron. Lett.*, vol 36, n10, pages 895-897, May 2000.
- [6] Z. Yun, M. F. Iskander, and Z. Zhang. A Fast Indoor/Outdoor Ray Tracing Procedure Using Combined Uniform Rectangular and Unstructured Triangular Grids. *Proc. IEEE AP-S Inte. Symp. Dig.*, pages 1134-1137, July 2000.
- [7] R. Hoppe, P. Wertz, G. Wlfl, and F.M. Landstorfer. Fast and Enhanced Ray Optical Propagation Modeling for Radio Network Planning in Urban and Indoor Scenarios. *MPRG Wireless Personal Communications Symposium*, Blacksburg (Virginia, USA), 14-16 June 2000.
- [8] S. F. Fortune, D. M. Gay, B. W. Kernighan, O. Landron, R. A. Valenzuela, and M. H. Wright. Wise design of indoor wireless systems: Practical computation and optimization. *IEEE Comput. Sci. Eng. Mag.*, pages 58-68, Spring 1995.
- [9] F. A. Agelet, F. P. Fontan, and A. Formella. Fast ray-tracing for microcellular and indoor environments. *IEEE Trans. Magn.*, 33:1484-1487, March 1997.
- [10] F. A. Agelet, A. Formella, J. M. H. Rabanos, F. I. de Vicente, and F. P. Fontan. Efficient ray-tracing acceleration techniques for radio propagation modeling. *IEEE-VEH*, 49:2089-2104, November 2000.
- [11] K. Rizk, J.-F. Wagen, and F. Gardiol. Two-dimensional ray-tracing modeling for propagation prediction in microcellular environments. *IEEE-VEH*, 46:508-518, May 1997.
- [12] G. E. Athanasiadou and A. R. Nix. A novel 3-D indoor ray-tracing propagation model: The path generator and evaluation of narrow-band and wide-band predictions. *IEEE-VEH*, 49:1152-1168, July 2000.
- [13] R.G. Kouyoumjian and P.H. Pathak. A uniform geometrical theory of diffraction for an edge in a perfectly conducting surface. *Proc. IEEE*, pages 1448-1461, November 1974.
- [14] P. Combeau. Simulation efficace et caractrisation du canal radiomobile en environnement rel. Application aux systemes sans fil. *PhD-Thesis*, University of Poitiers, France, 2004.
- [15] ITU. Multipath propagation and setting of its characteristics. Technical report, IUT, March 1999. Technical Report, Doc3/BL/2-F.
- [16] L. Aveneau, P. Combeau, R. Vauzelle, and M. Mériaux. Efficient computation of radio coverage zone using a spatial partitionment approach. Orlando, October 2003. VTC2003.
- [17] P. Combeau, L. Aveneau, R. Vauzelle, and C. Chatellier. Deterministic propagation model influence on a wireless digital transmission simulation in real environment. *PIMRC04*, Barcelona, September 2004.